7-25-2017

Origin of primitive ocean island basalts by crustal gabbro assimilation and multiple recharge of plume-derived melts

Anastassia Y. Borisova

Wendy A. Bohrson

Michel Grégoire

AGU PUBLICATIONS

Geochemistry, Geophysics, Geosystems

RESEARCH ARTICLE
10.1002/2017GC006986

Origin of primitive ocean island basalts by crustal gabbro assimilation and multiple recharge of plume-derived melts

Anastassia Y. Borisova[1,2], Wendy A. Bohrson[3], and Michel Grégoire[1]

[1]Géosciences Environnement Toulouse, Université de Toulouse, UPS OMP - CNRS - IRD, 14 Avenue E. Belin, 31400 Toulouse, France, [2]Geological Department, Lomonosov Moscow State University, Vorobievu Gory, 119899 Moscow, Russia, [3]Department of Geological Sciences, Central Washington University, Ellensburg, WA 98926, USA

Key Points:
- We employed the Magma Chamber Simulator (MCS) to constrain mechanisms of primitive ocean island basalt (OIB) genesis
- Our results highlight the important impact that crustal gabbro assimilation and mantle recharge events have on the geochemistry of OIBs
- The isotopic equilibrium between primitive OIB and associated deep plume mantle source(s) is the exception rather than the rule

Supporting Information:
- Table S1
- Data Set S1

Correspondence to:
A. Y. Borisova,
anastassia.borisova@get.omp.eu

Citation:
Borisova, A. Y., W. A. Bohrson, and M. Grégoire (2017), Origin of primitive ocean island basalts by crustal gabbro assimilation and multiple recharge of plume-derived melts, *Geochem. Geophys. Geosyst.*, *18*, 2701–2716, doi:10.1002/2017GC006986.

Received 27 APR 2017
Accepted 27 JUN 2017
Accepted article online 6 JUL 2017
Published online 25 JUL 2017

Abstract Chemical Geodynamics relies on a paradigm that the isotopic composition of ocean island basalt (OIB) represents equilibrium with its primary mantle sources. However, the discovery of huge isotopic heterogeneity within olivine-hosted melt inclusions in primitive basalts from Kerguelen, Iceland, Hawaii and South Pacific Polynesia islands implies open-system behavior of OIBs, where during magma residence and transport, basaltic melts are contaminated by surrounding lithosphere. To constrain the processes of crustal assimilation by OIBs, we employed the Magma Chamber Simulator (MCS), an energy-constrained thermodynamic model of recharge, assimilation and fractional crystallization. For a case study of the 21–19 Ma basaltic series, the most primitive series ever found among the Kerguelen OIBs, we performed sixty-seven simulations in the pressure range from 0.2 to 1.0 GPa using compositions of olivine-hosted melt inclusions as parental magmas, and metagabbro xenoliths from the Kerguelen Archipelago as wallrock. MCS modeling requires that the assimilant is anatectic crustal melts ($P_2O_5 \leq 0.4$ wt.% contents) derived from the Kerguelen oceanic metagabbro wallrock. To best fit the phenocryst assemblage observed in the investigated basaltic series, recharge of relatively large masses of hydrous primitive basaltic melts ($H_2O = 2–3$ wt%; MgO = 7–10 wt.%) into a middle crustal chamber at 0.2 to 0.3 GPa is required. Our results thus highlight the important impact that crustal gabbro assimilation and mantle recharge can have on the geochemistry of mantle-derived olivine-phyric OIBs. The importance of crustal assimilation affecting primitive plume-derived basaltic melts underscores that isotopic and chemical equilibrium between ocean island basalts and associated deep plume mantle source(s) may be the exception rather than the rule.

1. Introduction

The first *a priori* thesis of Chemical Geodynamics is isotopic equilibrium of oceanic basalts (mid-ocean ridge basalt and ocean island basalt, MORB and OIB, respectively) with their corresponding mantle sources [*Allegre*, 1982]. Isotopic signatures of oceanic magmas are ascribed to heterogeneity of mantle sources (major mantle "end-members": enriched mantle (EM), high-μ (HIMU), and depleted mantle (DMM)) [*Zindler and Hart*, 1986]. An impact from either crustal or mantle lithospheric assimilation is typically assumed to be negligible based on an old paradigm about the absence of any significant chemical and isotopic exchange between the primary oceanic melts and either crust or lithospheric mantle. The role of assimilation may be studied by multiple approaches, including using olivine- and chromite-hosted melt inclusions that are interpreted to represent a parental magma and therefore are witnesses to early-stage processes happening in lithospheric magma chamber(s) [*Sobolev et al*., 2011; *Borisova et al*., 2012, 2014; *Genske et al*., 2014]. Pb isotope compositions of olivine-hosted basaltic melts from a range of OIBs are impressively heterogeneous, and span between HIMU, DMM and EM components (Figure 1). The world-scale isotopic variations in the olivine-hosted melt inclusions from several investigated OIB samples imply that the existing isotopic systematics [e.g., *Zindler and Hart*, 1986] traditionally based on the bulk basalt compositions should be revised. In fact, a growing number of studies provides evidence for assimilation of lithosphere (mantle or crustal) by oceanic basalts, including mid-ocean ridge (MORB) and ocean island basalts (OIB) [e.g., *Hilton et al*., 1995; *Borisova et al*., 2001, 2002, 2012, 2014; *Kamenetsky et al*., 2001; *Kamenetsky and Gurenko*, 2007; *Bindeman et al*., 2006, 2008; *Genske et al*., 2014; *Olierook et al*., 2017]. Assimilation of lithosphere by oceanic magmas was suggested to happen through (a) assimilation of wallrock-derived partial melts [*Borisova et al*., 2002; *Gurenko and*

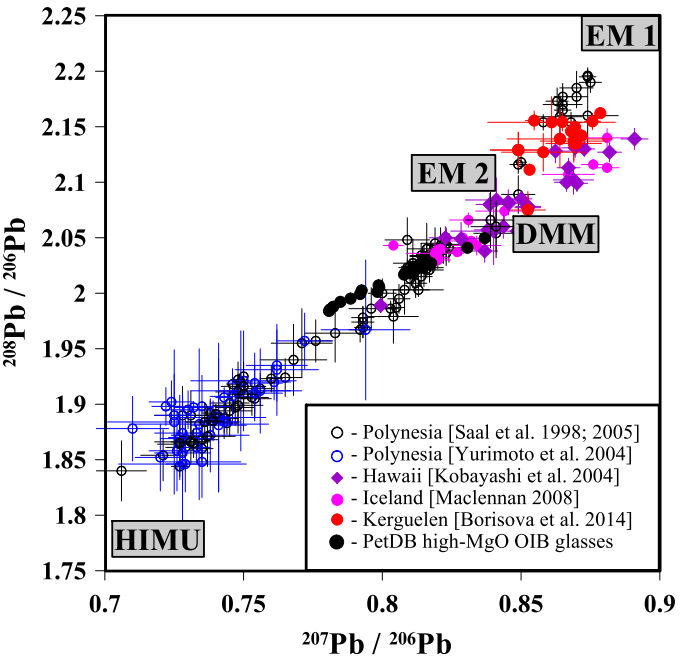

Figure 1. $^{208}Pb/^{206}Pb$ versus $^{207}Pb/^{206}Pb$ diagram illustrating previously investigated OIB olivine-hosted melt inclusions in comparison to EM-1, EM-2, DMM and HIMU mantle end-members. The mantle end-member compositions correspond to those of *Zindler and Hart* [1986]. The OIB melt inclusion data (Polynesia, Hawaii, Iceland, South Pacific and Kerguelen islands) with corresponding error bars are from *Saal et al.* [1998, 2005], *Yurimoto et al.* [2004], *Kobayashi et al.* [2004], *Maclennan* [2008], and *Borisova et al.* [2014]. The investigated 21–19 Ma Kerguelen plume-derived basalts (red points) have EM signatures. The effect of sample surface contamination discovered by *Paul et al.* [2011] has been taken into account during the Pb isotope analyses by LA-MC-ICP-MS [*Borisova et al.*, 2014]. The Kerguelen melts approaching DMM end-member are likely affected by depleted lithosphere due to localization of the corresponding hot spot near spreading centers [e.g., *Grégoire et al.*, 1997].

Sobolev, 2006; *Kvassnes and Grove*, 2008], (b) dissolution of crustal minerals into OIB melts [*Edwards and Russell*, 1998; *Borisova et al.*, 2014], as well as (c) multistage interaction between oceanic basalt with hydrous lithospheric mantle at the oceanic Moho levels [*Borisova et al.*, 2012]. Troctolite assimilation by MORB leads the liquid line of descent to the plagioclase–olivine saturation boundary, producing primitive troctolites [*Kvassnes and Grove*, 2008]. Moreover, a growing number of studies provides strong evidence for anomalously ancient (from 660 Ma to 3.0 Ga) lithosphere beneath oceanic islands [e.g., *Borisova et al.*, 2001; *Yano et al.*, 2011; *Torsvik et al.*, 2013, 2015; *Ashwal et al.*, 2017], suggesting the composition of these OIB (especially those located in the Dupal isotopic anomaly [e.g., *Hart*, 1984] regions) to be affected by the lithosphere. It was recently suggested that the EM-type OIBs related to activity of the Kerguelen plume can be explained by production of olivine-saturated melts with high K_2O/P_2O_5 and Al_2O_3/TiO_2 through selective dissolution of plagioclase from wallrock metagabbro during the assimilation process [*Borisova et al.*, 2002, 2014]. However, the impact of crustal assimilation on primitive ocean island basalt chemistry is still uncertain.

The case study presented here uses a 21–19 Ma Kerguelen plume-derived basaltic series possessing EM isotopic compositions; significantly, it is the most primitive (MgO = 7–10 wt.% in the homogenized basaltic melts) series ever found among the Kerguelen plume-derived OIB [e.g., *Borisova et al.*, 2002]. The fact that the 21–19 Ma primitive OIB series has lowest $^{206}Pb/^{204}Pb$ ratios, Th, Nb and Ta depletion and Pb enrichment in the primitive mantle-normalized pattern, resembling those of Cretaceous Kerguelen Plateau basalts has been considered as evidence for the lithospheric [*Borisova et al.*, 2002], in particular, crustal [*Borisova et al.*, 2014] assimilation. Moreover, high $K_2O/P_2O_5 \geq 4.7$ and $Al_2O_3/TiO_2 \geq 4.3$ found the olivine phenocryst-hosted melt inclusions were interpreted as crustal assimilant melts generated upon interaction between wallrock gabbro crust and the parental basaltic magma. We address the question of crustal assimilation through thermodynamic modeling of the primitive olivine basalt series related to the Kerguelen plume. Physical and chemical data on fluid, solid and melt inclusions [e.g., *Borisova et al.*, 2002, 2014] and metagabbro xenoliths [e.g., *Grégoire et al.*, 1994, 1998] coupled with energy-constrained open-system thermodynamic modeling using the Magma Chamber Simulator [*Bohrson et al.*, 2014] make it now possible to constrain a mechanism of crustal assimilation by OIB.

2. Geological Background and Thermodynamic Approach

2.1. Kerguelen Plume Activity and Primitive Basalt Chemistry

Magmatism of the Kerguelen plume [*Frey et al.*, 2015; *Sushchevskaya et al.*, 2015; *Olierook et al.*, 2017] is represented by construction of the Cretaceous Kerguelen Plateau (118–85 Ma) and the subsequent formation of the Kerguelen Archipelago and Heard Island (39–0.1 Ma) as well as a seamount (21–19 Ma) located

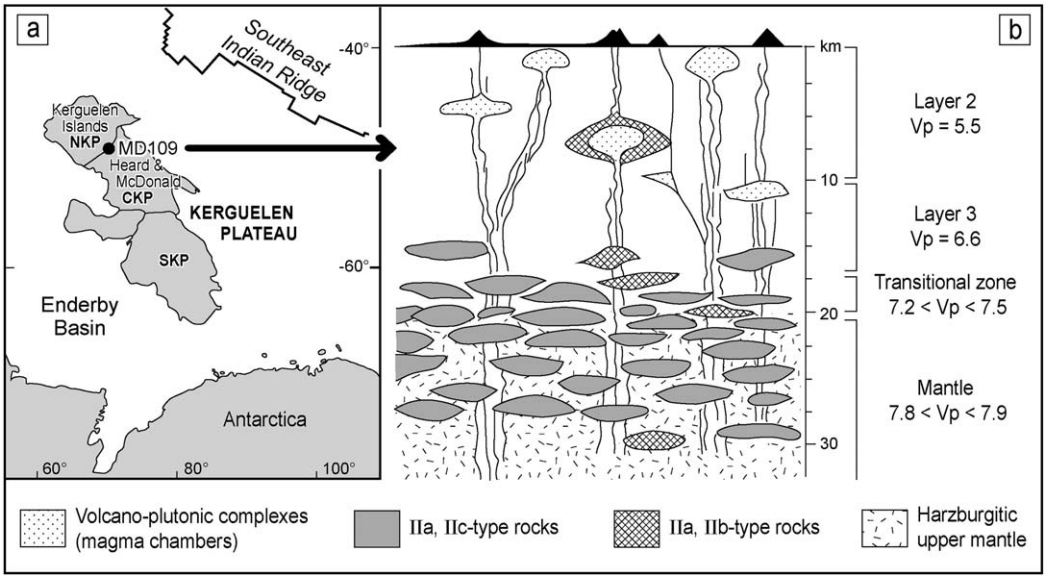

Figure 2. (a) Inset map of the Indian Ocean structures related to the Kerguelen plume activity and, (b) schematic geologic structure of the MD 109 lithosphere. The map illustrates the Kerguelen Plateau (Northern, NKP; Central, CKP and Southern, SKP), Kerguelen Islands (or Kerguelen Archipelago), Heard and McDonald islands and the MD 109 seamount (21–19 Ma basalt series) sampled by research vessel "Marion Dufresne" team by dredging. Seismic P-wave velocities (Vp, km s^{-1}) in the "Layer 2," "Layer 3," "Transitional zone" and "Mantle" correspond to those investigated by *Grégoire et al.* [1998, 2001]. The "Volcano-plutonic complexes (magma chambers)," "IIa- and IIc-type rocks," "IIa and IIb-type rocks" and "Harzburgitic upper mantle" correspond to the schematic locations of the magma chambers, IIa- and IIc-type, IIb-type xenolith rocks and harzburgitic mantle, respectively, in the MD 109 Kerguelen lithosphere [*Grégoire et al.*, 1998, 2001].

between the Kerguelen Archipelago and Heard Island (Figure 2). The Kerguelen Archipelago was built by interaction between the South East Indian Ridge (SEIR) and the Kerguelen plume beginning 39 Ma ago [*Gautier et al.*, 1990; *Grégoire et al.*, 1997; *Weis et al.*, 2002] that produced a large volume of tholeiitic and transitional magma. The subsequent migration of the SEIR northward away from the plume resulted in Archipelago magmas becoming more alkaline [e.g., *Gautier et al.*, 1990; *Frey et al.*, 2000; *Nicolaysen et al.*, 2000]. The 29–24 Ma flood tholeiitic basalts and metagabbros of the Kerguelen Archipelago are considered to be derived from the plume mantle [e.g., *Frey et al.*, 2002a,b; *Weis et al.*, 2002]. In addition, Sr–Nd–Pb isotope compositions of the 25–22 Ma Archipelago transitional and alkaline basalts are also attributed to the associated Kerguelen plume [*Weis and Frey*, 2002]. However, some Kerguelen mafic volcanic products, such as the 21–19 Ma olivine-rich basaltic series, sampled during the "Marion Dufresne" MD 109 cruise (MD109; Figure 2), have Pb isotope signatures distinct from the 25 to 22 Ma Kerguelen plume mantle-derived basalts [*Frey et al.*, 2002b; *Weis et al.*, 2002], a feature that was attributed to lithospheric assimilation [*Borisova et al.*, 2002, 2014]. Dredge 6 (D6, collected >1 ton of very fresh samples, mainly pillow basalts with abundant olivine phenocrysts) was on a flank of the 21–19 Ma seamount between the Northern and Central Kerguelen Plateau (NKR and CKP, Figure 2). *Borisova et al.* [2014] demonstrated that the major element and Pb isotope chemistry of the parental basalt magma revealed by olivine phenocryst-hosted basaltic melt inclusions and the host olivine (21 Ma sample number MD109-D6–87) is related to crustal assimilation through binary mixing of Plume and Assimilant melts characterized by contrasting TiO_2 and P_2O_5 contents, and corresponding contrasting K_2O/P_2O_5 and Al_2O_3/TiO_2 ratios (Table 1, Figures 3 and 4).

P_2O_5-rich Plume melts with P_2O_5 contents of 0.5–3.8 wt.% (Table 1 and Figure 3) are hosted in olivine ($Fo_{83–86}$) and represent the major type of the melt inclusions. The melt inclusions have low K_2O/P_2O_5 ($\leq$ 4) and Al_2O_3/TiO_2 ($\leq$4.2) ratios at high TiO_2 ($\geq$3.0 wt.%) and MgO contents (7–10 wt.%) (Figures 3 and 4). The Plume melt inclusions show variable Pb isotope ratios ($^{207}Pb/^{206}Pb = 0.838–0.877$) and ($^{208}Pb/^{206}Pb = 2.075–2.154$), which overlap those of the host D6 and contemporaneous Kerguelen plume-derived basalts [*Borisova et al.*, 2014]. Pb isotope compositions interpreted as Plume melts demonstrate significant dispersion around the 25–22 Kerguelen plume composition (Figure 4). The second important type of melt inclusion represents the Assimilant melts hosted by olivine $Fo_{82–83}$ (Table 1). High K_2O/P_2O_5 ($\geq$4.7) and Al_2O_3/TiO_2 ($\geq$4.3) ratios in the melt inclusions representing Assimilant in Figure 4 are due to low P_2O_5 ($\leq$0.4 wt.%)

Table 1. Major, Trace Element and Pb Isotope Compositions of the 21–19 Ma Kerguelen MD 109 Host Basalt Series, Olivine-Hosted Melt Inclusions, Hypothesized Crustal Assimilant, and 25–22 Ma Kerguelen Plume

	Plume[a]	Assimilant[a]	Model Crustal Assimilant[a]	Host Basalt Series	Kerguelen Plume[b]
Fo (mol%)[c]:	79; 82–86	82–83		78–85	
Pressure (GPa)[d]:	≤0.1–0.3	~ 0.2			
Temperature (°C):	1195–1233	1190–1233			
SiO_2 [h e] (wt.%):	49.0 ± 2.6	49.5 ± 1.1	50–52	46.52	
TiO_2 [h]:	3.5 ± 0.4	2.8 ± 0.1	3.3–3.4	2.12	
Al_2O_3 [h]:	12.9 ± 1.1	13.4 ± 0.6	15–17	8.56	
FeO [h]:	9.7 ± 1.1	10.1 ± 1.0	11–12	11.87	
MgO [h]:	7.6 ± 2.1	7.2 ± 0.1	6–7	20.16	
CaO [h]:	11.1 ± 1.1	10.9 ± 1.3	6.4–8.4	7.39	
Na_2O [h]:	2.4 ± 0.2	2.4 ± 0.1	3.0–3.6	1.49	
K_2O [h]:	1.8 ± 0.5	2.2 ± 0.4	2.5–3.3	1.45	
P_2O_5 [h]:	1.0 ± 0.9	0.35 ± 0.12	0.2–0.4	0.36	
K_2O/P_2O_5[e]	2.7 ± 1.2	7.2 ± 4.4	4.4–13.9	3.9–4.0	0.8–4.6
Al_2O_3/TiO_2[e:]	3.7 ± 0.5	4.8 ± 0.4	4.4–5.1	4.0–4.1	4.3–4.5
$(La/Sm)_n$[f]	2.2–4.5		1.4–3.0	4.75	
$^{207}Pb/^{206}Pb$ average[e]	0.855 ± 0.017	0.859 ± 0.006	0.87–0.88	0.8691–0.8694	0.837–0.846
$^{208}Pb/^{206}Pb$ average[e]	2.126 ± 0.027	2.120 ± 0.016	2.14–2.18	2.1408–2.1415	2.112–2.118

[a]"Plume," "Assimilant," correspond to average major, trace element and Pb isotope compositions (± 2σ S.D. representing melt heterogeneity) of the 21 Ma olivine-hosted homogenized melt inclusions. Theoretical assimilant end-member called "Model Crustal Assimilant" is hypothesized in the work of *Borisova et al*. [2014], which suggests that the fraction of Model Crustal Assimilant is higher than 0.5, meaning that at least 50% of the mass of the contaminated parental magma is attributed to a crustal source. All compositions are from *Borisova et al*. [2014].

[b]Kerguelen Plume composition corresponds to that of the 25–22 Ma Kerguelen plume-derived OIBs according to data of *Frey et al*. [2002b], *Weis and Frey* [2002] and *Borisova et al*. [2014] and references therein.

[c]Fo is the forsteritic content of the host olivine for melt inclusions.

[d]Pressure corresponds to pressure estimated based on CO_2 density in the olivine-hosted fluid inclusions. Temperature ranges correspond to those obtained experimentally from the olivine-hosted inclusion homogenization [*Borisova et al*., 2002, 2014].

[e]"h" superscript means that average major element composition of the melt inclusions corresponds to the composition of the homogenized melt inclusions of the "Plume," "Assimilant" melt components defined in *Borisova et al*. [2014]. FeO content in the host basalts is recalculated from *Borisova et al*. [2002]. "average" superscript means average Pb isotope composition of the "Plume," "Assimilant" melts [*Borisova et al*., 2014].

[f]Trace element ratios are normalized to the composition of primitive mantle of *Sun and McDonough* [1989]. The trace element data on the "Plume" melt inclusions are adapted from *Borisova et al*. [2002].

and TiO_2 (≤2.9 wt.%) at MgO contents of 7–8 wt.% (Figure 3). This type displays higher K_2O/P_2O_5 and Al_2O_3/TiO_2 ratios relative to those of the host basalt (Table 1 and Figure 4). Because of low P_2O_5 and TiO_2 contents and corresponding high K_2O/P_2O_5 and Al_2O_3/TiO_2 ratios, the Assimilant melts are unlike Kerguelen plume-derived melts or melts derived from deep mantle [*McDonough and Sun*, 1995]. The P_2O_5-poor compositions require melt derivation from a wallrock gabbro [*Borisova et al*., 2014]. The Assimilant inclusions with these major element characteristics display Pb isotopic ratios of $^{207}Pb/^{206}Pb$ (0.853–0.867) and $^{208}Pb/^{206}Pb$ (2.110–2.139), which are overlapping those of the host basalt and the associated basalts related to the Kerguelen plume [*Weis et al*., 2002; *Borisova et al*., 2002].

H_2O and CO_2 contents were not analyzed in the homogenized inclusions because of regular volatile loss during the homogenization experiment [e.g., *Danyushevsky et al*., 2002], although preliminary data on summary H_2O and CO_2 contents in glassy (i.e., naturally quenched) melt inclusions have been obtained by electron microprobe [*Borisova et al*., 2002]. These data suggest total volatile ($H_2O + CO_2$) contents in the basaltic melt reaching a of maximum 2.6 wt.%, although higher volatile, in particular water, contents may be expected in the primitive plume-derived magmas [e.g., *Xia et al*., 2016]. Because the investigated basaltic melts are primitive (not far from equilibrium with mantle), but resided in the crust at 6–9 km, *Borisova et al*. [2014] developed a geochemical model, according to which the basaltic melts accumulating in the parental magmatic chamber (a) were initially derived from heterogeneous Kerguelen plume. (b) The parental magma was strongly contaminated (through the wallrock partial melting or dissolution of wallrock plagioclase, generating the Assimilant melts) during the magma residence in the thick plagioclase-rich crust, and the produced melts (c) were progressively mixed during magma residence and transport to the surface. The crustal assimilation in the parental magma chamber proposed by *Borisova et al*. [2014] thus happens through binary mixing of Plume and Assimilant melts. To provide constraints on the process of assimilation, a

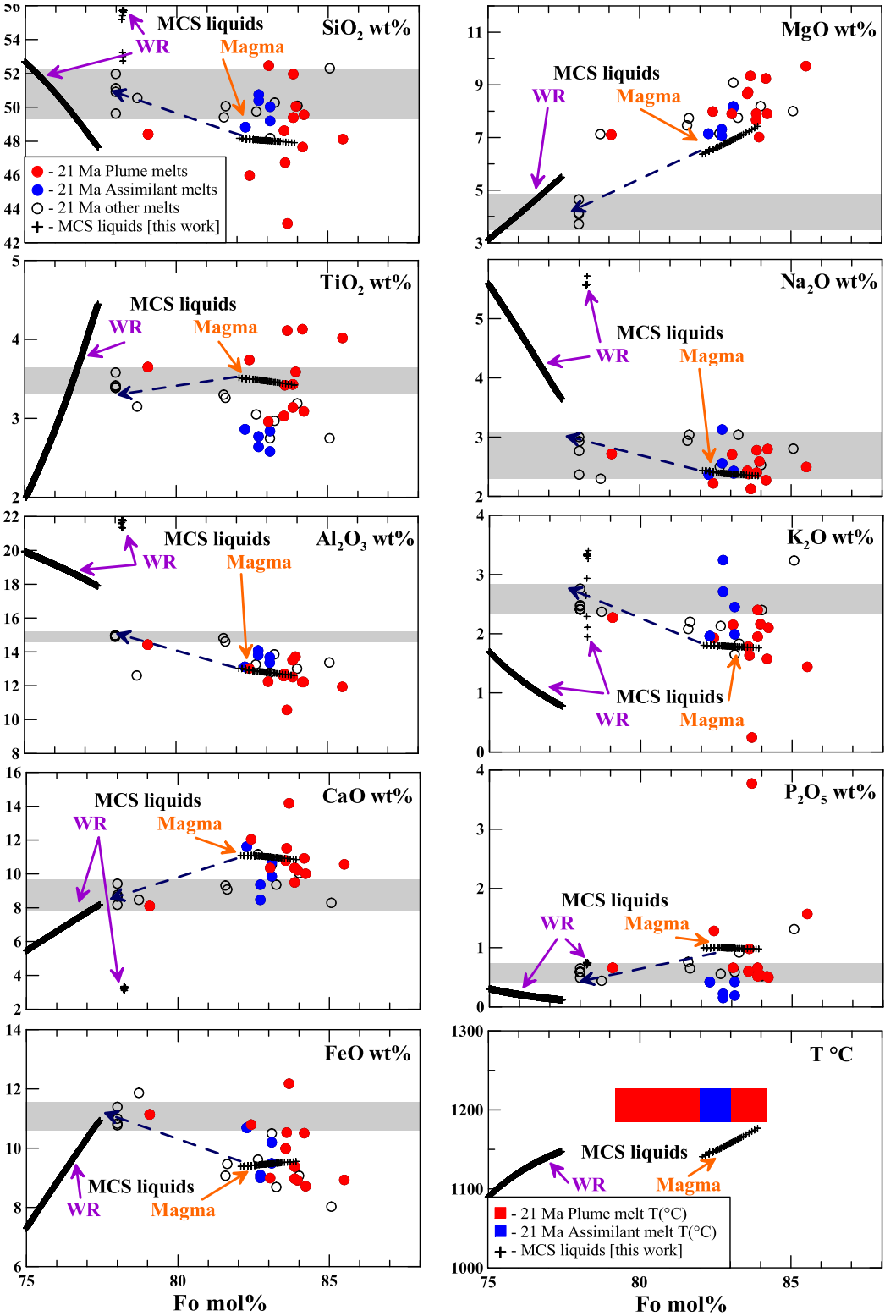

Figure 3. Major element contents and homogenization temperature measured for the olivine-hosted melt inclusions of the 21–19 Ma Kerguelen basaltic series versus corresponding forsterite (Fo, mol.%) content in the host olivine (or theoretically equilibrium olivine for the groundmass glass). The compositions of the basaltic melt inclusions are compared to those of the host basalts and the basaltic groundmass (matrix) glasses (grey field). "21 Ma Plume melts," "21 Ma Assimilant melts" and "21 Ma other melts" correspond to Plume, Assimilant melts and all other types of basaltic melts (e.g., matrix glasses and melt inclusions), respectively, according to *Borisova et al.* [2002, 2014]. The dashed arrows indicate the effect of crustal assimilation on the composition of the 21–19 Ma Kerguelen OIB basaltic series. The Magma Chamber Simulator (MCS) wallrock (WR) and the parental magma (Magma) liquids of one of the best fit 28w model are also demonstrated.

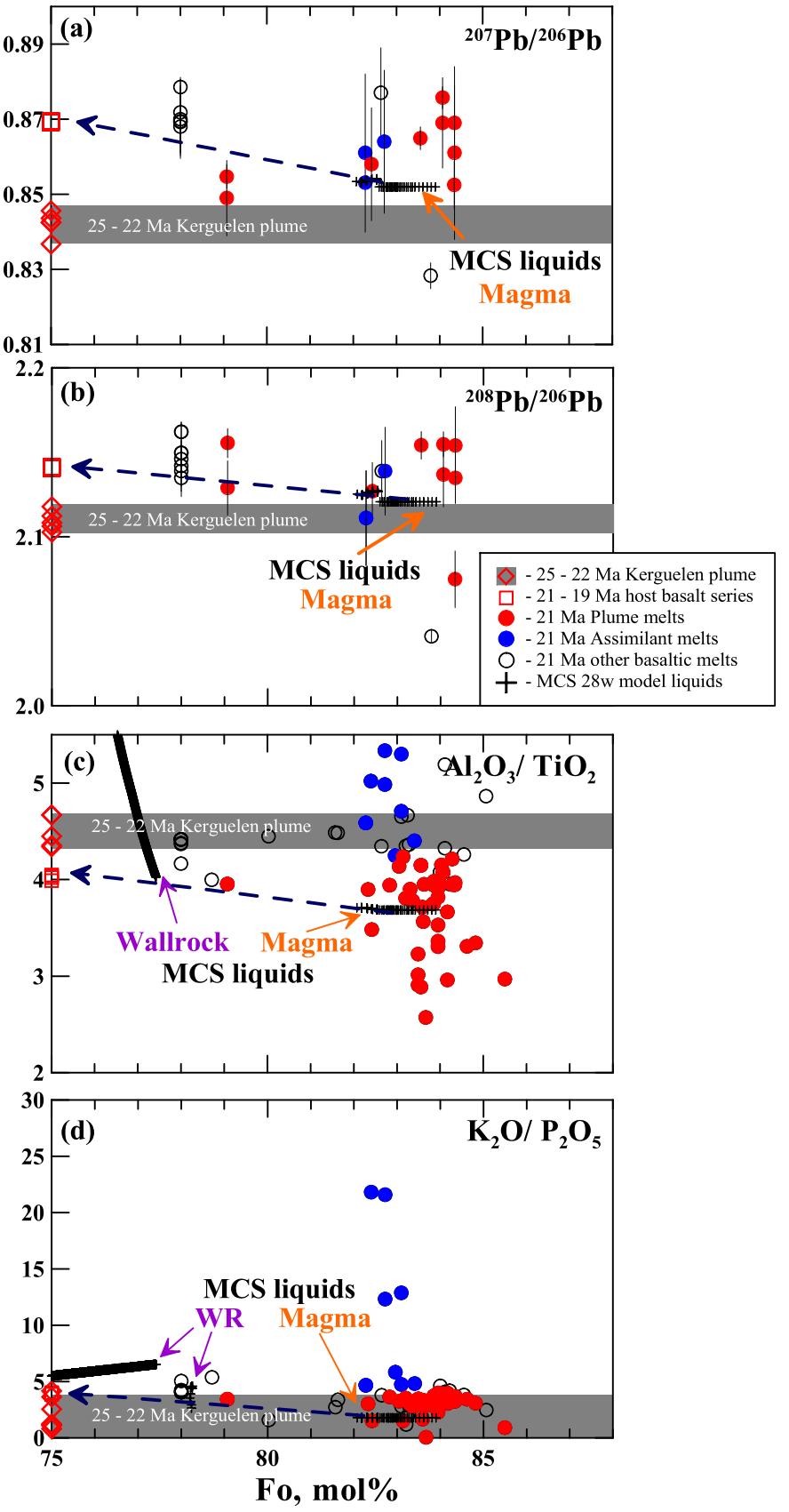

Figure 4. (continued)

theoretical assimilant end-member called Model Crustal Assimilant was estimated through binary mixing modeling. However, the previous models were not thermodynamically constrained.

2.2. Kerguelen Oceanic Crust and Upper Mantle

Overlapping ages of igneous rocks and similar geological history of the MD109 seamount (21–19 Ma) and the Kerguelen Archipelago (39–7 Ma Kerguelen Islands constructed on the North to Central Kerguelen Plateau) suggest similar geologic structure of the oceanic crust and upper mantle (Figure 2). 25–7 Ma alkaline lavas from the Kerguelen Archipelago (Kerguelen Islands) contain abundant ultramafic and mafic xenoliths including typical mantle xenoliths (type I) and magmatic products (type II) [*Grégoire et al*., 1994, 1998, 2001; *Mattielli*, 1996; *Mattielli et al.* 1999] with numerous gabbros and metagabbros indicating that melt/gabbro reaction processes likely occur. Type II xenoliths have been subdivided by *Grégoire et al*. [1994, 1998] into three mineralogical subtypes. Subtype IIa always contains clinopyroxene (Cpx), orthopyroxene (Opx) and spinel (Sp) and shows a regular modal evolution from ultramafic to mafic rocks such as metagabbros with or without garnet and sapphirine (Table 2). Subtype IIb is clinopyroxenites (Cpx + ilmenite (Ilm) + Sp) with or without garnet (Gr) and Sp + Ilm ± Gr metagabbros. The third subtype (IIc) is represented by Cpx + Ilm + Gr-bearing metagabbros. The oceanic crust of the Kerguelen Archipelago is not a typical oceanic crust. Indeed, it is very thick (15–20 km) and does not display a typical Moho discontinuity but a progressive one related to magmatic underplating process [*Recq et al*., 1990]. The Kerguelen oceanic crust was built through the interaction of the Southeast Indian Ridge (SEIR), the Kerguelen mantle plume and the Cretaceous plateau lithosphere [e.g., *Borisova et al*., 2002] a process that happened about 40 million years ago and characterized by an early intense tholeiitic-transitional magmatic activity [*Gautier et al*., 1990]. In such a scheme, the Kerguelen type IIa and IIb xenoliths correspond to those after *Grégoire et al*. [1994, 1998, 2001] to, respectively, tholeiitic-transitional cumulates and frozen melts more or less metamorphosed (granulite facies) and emplaced within the crust, the crust-mantle boundary and the upper mantle. After this construction stage, the evolution of the Kerguelen Islands continued in an intraplate setting and was characterized by an alkaline magmatism. The type IIb xenoliths are cumulates more or less metamorphosed related to this magmatic activity and emplaced within the Kerguelen crust, crust-mantle boundary and upper mantle. Formation of subtype IIa (cumulates) and IIc xenoliths (frozen melts) was related to crystallization of early tholeiitic-transitional magmatic intrusions, whereas subtype IIb are alkaline cumulates, some of which formed within the upper mantle (garnet-bearing rocks) [*Grégoire et al*., 1998]. The 25–7 Ma alkaline IIb-type cumulates are the most likely to represent the wallrock for the 21 Ma Kerguelen plume-derived basaltic melts because the early cumulates of alkaline magma were likely created as feeding channels for the repetitive pulses of the magma from the upper mantle through the crust. In this work, we use thermodynamic modeling to examine the efficacy of all II-type (IIa, IIb, IIc) metagabbro xenoliths as partially melted wallrock to explain the chemistry of basaltic melt inclusions and the mineralogy of the host phenocryst minerals found in the 21 Ma Kerguelen plume-derived basalt dredged on a flank of the seamount between the Northern and Central Kerguelen Plateau (NKP and CKP) (Figure 2).

2.3. Energy-Constrained Thermodynamic Modeling: The Magma Chamber Simulator

To understand how crustal assimilation and magma recharge can affect the parental basaltic magma, we performed numerical simulations of energy-constrained recharge, assimilation and fractional crystallization (RAFC) using the Magma Chamber Simulator (MCS), which models the elemental, isotopic, phase equilibria, mass and thermal evolution of a magma body undergoing recharge, assimilation, and fractional crystallization. As an estimate of the initial magma chamber liquid, we have used the average composition of Plume melt inclusions (Table 1) [*Borisova et al*., 2014]. Wallrock is represented by six metagabbro xenolith

Figure 4. (a-d). $^{207}Pb/^{206}Pb$, $^{208}Pb/^{206}Pb$, Al_2O_3/TiO_2 and K_2O/P_2O_5 measured in olivine phenocryst-hosted melt inclusions of the 21–19 Ma Kerguelen basaltic series versus corresponding forsterite (Fo, mol.%) content in the host olivine (or theoretically equilibrium olivine for the groundmass glass). The isotopic (with corresponding error bars) and major element compositions of the basaltic melt inclusions are compared to those of the host basalts and the 25–22 Ma Kerguelen plume-derived basalts (grey field). "21 Ma Plume melts," "21 Ma Assimilant melts" and "21 Ma other basaltic melts" correspond to Plume, Assimilant melts and all other types of basaltic melts (e.g., groundmass melts and other melt inclusions), respectively, according to *Borisova et al*. [2002, 2014]. The dashed arrows to higher values of $^{208}Pb/^{206}Pb$ and $^{207}Pb/^{206}Pb$, Al_2O_3/TiO_2 and K_2O/P_2O_5 indicate the effect of crustal assimilation on the composition of the 21–19 Ma Kerguelen OIB basaltic series. The Magma Chamber Simulator (MCS) wallrock (WR) and the parental magma (Magma) liquids of one of the best fit 28w model are demonstrated. The Pb isotope composition of the Magma liquids with corresponding olivine composition (Fo, mol.%) are those attributed to the Kerguelen Plume composition (Table 1).

Table 2. Initial Conditions for the Best-Fit Magma Chamber Simulator Models

Model	Model 15	Model 18	Model 22	Model 23w	Model 24w	Model 28w	Model 34w
Pressure (GPa)	0.2	0.2	0.2	0.2	0.2	0.3	0.2
Initial melt (liquidus T°C)	Plume[a] (1168)	Plume (1168)	Plume (1168)	Plume (1168)	Plume (1168)	Plume (1175)	Plume (1168)
Initial H_2O, wt.%	2.0	2.0	2.0	3.0	3.0	3.0	3.0
WR used[b]	GM 139	MG 134	MG 134	MG 134	MG 134	MG 134	GM 139
Xenolith type[b]	IIb	IIb	IIb	IIb	IIb	IIb	IIb
Xenolith mineralogy[b]	clinopyroxenite (Cpx, Ilm, Sp, Gr)	metagabbro (Plag, Cpx, Ilm, Sp)	metagabbro (Plag, Cpx, Ilm, Sp)	metagabbro (Plag, Cpx, Ilm, Sp)	metagabbro (Plag, Cpx, Ilm, Sp)	metagabbro (Plag, Cpx, Ilm, Sp)	clinopyroxenite (Cpx, Ilm, Sp, Gr)
Recharge events	1	1	4	3	4	4	4
Magma:recharge mass ratio[c]	1:1	1:1	1:1	1:1	1:1	1:1	1:1
Recharge magma	Plume[a]	Plume	Plume	Plume	Plume	Plume	Plume
Magma T at recharge, °C	1130	1130	1137–1140	1138–1140	1137–1140	1152–1155	1137–1140
Model:	Model 15p	Model 15w	Model 52w	Model 51w	Model 45w	Model 48w	Model 38w
Pressure (GPa)	1.0	0.2	0.2	0.2	0.2	0.2	0.2
Initial melt (liquidus T °C)	Plume (1250)	Plume (1168)	Plume (1168)	Plume (1168)	Plume (1168)	Plume (1168)	Plume (1168)
Initial H_2O, wt.%	3.0	3.0	3.0	3.0	3.0	3.0	3.0
WR used[a]	GM 139	GM 139	MG 14	DR 6.5	ARC 343	ARC 343	GM 419
Xenolith type[a]	IIb	IIb	IIb	IIa	IIa	IIa	IIc
Xenolith mineralogy[a]	metagabbro (Plag, Cpx, Ilm, Sp)	metagabbro (Plag, Cpx, Ilm, Sp)	clinopyroxenite (Cpx)	pyroxene metagabbro (Cpx, Plag)	metagabbro (Plag, Cpx, Gr, Sa)	metagabbro (Plag, Cpx, Gr, Sa)	metagabbro (Plag, Cpx, Ilm, Gr)
Recharge events	1	4	4	4	4	4	4
Magma:recharge mass ratio[c]	1:1	1:1	1:1	1:1	1:1	1:0.75	1:1
Recharge magma	Plume	Plume	Plume	Plume	Plume	Plume	Plume
Magma T at recharge, °C	1175	1127–1130	1127–1130	1127–1130	1132–1135	1132–1135	1137–1140

[a]Plume is average composition of Plume melt (Table 1) used for the MCS modeling as initial melt/magma and as recharge melt/magma.
[b]WR used–wallrock sample numbers correspond to those of the Kerguelen Archipelago mafic (II-type) xenoliths. Xenolith type and mineralogy data are from *Grégoire* et al. [1994, 1998]. Cpx–clinopyroxene, Plag–plagioclase, Gr–garnet, Sp–spinel, Sa–sapphirine, Ilm–ilmenite.
[c]Magma mass refers to initial mass of magma. For example, a mass ratio of 1:1 indicates that the initial magma body mass and the mass of recharge magma were the same. A mass ratio of 1, for 4 events, yields a total mass of recharge magma added of 4 times that of the initial magma body mass.

compositions (IIa-, IIb-, IIc-types), although we focused mostly on the IIb-type metagabbros because they are the most representative of crustal wallrock created by repetitive pulses of the alkaline OIB magma through the lithosphere to the surface [*Grégoire et al*., 1994, 1998, 2001]. For the modeling, the following initial conditions have been assumed: Fe_2O_3/FeO ratio = 0.24 [*Borisova et al*., 2002], and water content in the initial Plume melt varies from 2 to 3 wt. % in accordance with moderate contents reported by experimental work on basaltic melt inclusions and mafic cumulates [*Borisova et al*., 2002; *Freise et al*., 2009; *Scoates et al*., 2008]. Pressure was set from 0.2 to 0.3 GPa in accordance with the density of olivine-hosted fluid inclusions [*Borisova et al*., 2002, 2014]. One model (15p) was performed at 1.0 GPa because IIb-type metagabbro xenoliths are interpreted to represent mafic magma cumulates that were equilibrated in the deep lithosphere through formation of dominantly high-pressure metamorphic assemblages and textures (Figure 2) [*Grégoire et al*., 1994, 1998, 2001]. In all of the MCS simulations, a percolation threshold ($f_{l,crit}^{WR}$) required for transfer of wallrock liquid in the magma body was set to 0.08 (8%); see *Bohrson et al*. [2014] for further discussion of this threshold and its limits. Zero to four recharge/magma mixing events were modeled using the Plume melt composition as the recharge end-member. Sixty-seven successful simulations (see supporting information Table S1 and Data Set S1) were performed, with results evaluated based on their ability to reproduce the olivine-dominated host basalt mineralogy and the major element compositions of Plume and Assimilant melts [*Borisova et al*., 2014]. In the following text the "melts" correspond to the natural system investigated by using melt inclusions and the "liquids" are those modeled by the Magma Chamber Simulator code.

3. Magma Chamber Simulator Results and Discussion: Effective Crustal Gabbro Assimilation Accompanied by High Mass Rates of Recharge

3.1. Magma Chamber Simulator Results Pertaining to Basalt Mineralogy

The goal of the MCS modeling was to reproduce the major element composition of assimilant (which is based on the average composition of the olivine-hosted Assimilant melt inclusions), as well as the olivine-dominated mineralogy observed in the basaltic series. The 21 Ma Kerguelen basalt consists of ~97 vol.%

Table 3. Extended Results of Best-Fit Magma Chamber Simulator Models[a]

Model	Model 15	Model 18	Model 22	Model 23w	Model 24w	Model 28w	Model 34w
T solidus WR, °C	775	900	900	900	900	855	775
Mass of Ol accumulated in magma (Fo, mol.%)	7	7	16 (81–83)	15 (81–84)	15 (82–84)	14 (82–84)	21 (81–84)
Mass of Cpx accumulated in magma	35	18	0	0	0	0	0
Cumulative liq.WR added to magma	16	1	6	4	4	6	18
SiO_2 liq.WR, wt.%	56–69	53–56	49–56	51–56	50–56	48–54	53–69
TiO_2 liq.WR	0.4–2.2	0.6–3.1	0.6–5.1	0.6–4.1	0.6–4.4	0.5–4.4	0.4–2.8
Al_2O_3 liq.WR	15–18	18–21	17–21	17–21	17–21	18–21	15–18
K_2O liq.WR	0.8–3.6	1.3–3.3	0.7–3.3	1.0–3.3	0.9–3.3	0.8–3.3	0.6–3.6
P_2O_5 liq.WR	0.05–0.4	0.2–0.8	0.1–0.8	0.9–4.8	0.1–0.8	0.6–0.1	0.04–0.4
SiO_2 liq.M, wt.%	48–52	48–49	48–49	48	48	48	48–49
TiO_2 liq.M	2.6–3.6	3.5–3.7	3.5–3.6	3.4–3.5	3.4–3.5	3.4–3.5	3.4–3.5
Al_2O_3 liq.M	12–16	13–14	12.8–13.2	12.6–13.1	12.6–13.0	12.6–13.0	12.6–13.3
K_2O liq.M	1.8–2.3	1.8–2.0	1.8	1.8	1.8	1.8	1.8
Magma phases (cumulative mass)	Cpx (35), Ol (7), Ilm (7), Sp (4.2)	Ol (7), Cpx (18)	Ol (16)	Ol (15)	Ol (15)	Ol (14)	Ol (21)
WR phases (cumulative mass for major phases) Resulting WR	Cpx (35), Flds (18), Opx (17), Ilm (7) gabbro	Cpx (41), Flds (26), Ol (6), Opx(6), Opx (14), Ilm (3) gabbro	Apt, Bi, Cpx (39), Flds (25), Ol (7), Opx (11), Ilm (2.9), Sp, W gabbro	Apt, Bi, Cpx (40), Flds (26), Ol (6), Opx (12), Ilm (3), Sp, W gabbro	Apt, Bi, Cpx (40), Flds (25), Ol (6), Opx (12), Ilm(3), Sp, W gabbro	Apt, Bi, Cpx (43), Flds (21), Hb, Ol(2.4), Opx(17), Ilm(1.2), Sp, W gabbro	Amph, Apt, Bi, Cpx(34), Flds(17), Opx(16), Qtz, Ilm(7), W gabbro
T magma final, °C	1081	1111	1140	1121	1130	1141	1110
Model:	Model 15p	Model 15w	Model 52w	Model 51w	Model 45w	Model 48w	Model 38w
T solidus WR, °C	1065	775	925	940	930	930	770
Mass of Ol accumulated in magma (Fo, mol.%)	0 -	22 (81–84)	20 (81–84)	20 (81–84)	20 (81–84)	18	22 (81–84)
Mass of Cpx accumulated in magma	58	0	0	0	0	7	2
Cumulative liq.WR added to magma	1.8	18	31	22	16	16	19
SiO_2 liq.WR, wt.%	48–63	48–69	45–57	48–52	51–52	51–52	50–62
TiO_2 liq.WR	3.8–7.0	0.4–3.4	0.6–1.7	0.1–0.3	0.1–0.6	0.1–0.6	0.4–3.0
Al_2O_3 liq.WR	14.9–17.0	12.6–18.2	12.6–23	22–24	22–24	22–23	17–19
K_2O liq.WR	2.9–3.2	0.6–3.6	0.05–2.5	0.1–1.9	1.7–3.3	1.5–3.2	0.2–2.0
P_2O_5 liq.WR	0.3–1.2	0.04–1.0	0.01–0.8	0.01–0.8	0.04–0.3	0.03–0.3	0.1–1.0
SiO_2 liq.M, wt.%	48–50	48–49	48	48	48	48–49	48–49
TiO_2 liq.M	2.7–3.9	12.6–13.0	3.4–3.5	3.4–3.5	3.4–3.5	3.4–3.5	3.4–3.5
Al_2O_3 liq.M	12.6–16.9	3.4–3.5	12.6–13.7	12.6–13.6	12.6–13.4	12.6–13.8	12.6–13.4
K_2O liq.M	1.8–2.8	1.8	1.8	1.8	1.8	1.8–1.9	1.8
Magma phases (cumulative mass)	Apt (1.7), Cpx (58), Opx (6), Ilm (4)	Ol (22)	Ol (20)	Ol (20), Cpx, Sp	Ol (20)	Ol (18), Cpx (7), Sp	Ol (22), Cpx (2)
WR phases (cumulative mass for major phases) Resulting WR	Cpx (39), Flds (26), Gr, Opx (18), Qtz, Ilm, Wtl granulite	Amph, Apt, Bi, Cpx (34), Flds (16), Qtz, Opx (16), Ilm (7), W gabbro	Cpx (50), Flds (38), Ol (12) gabbro	Apt, Bi, Cpx, Flds (39), Hb, Ol (14), Opx, Sp (0.19), W gabbro	Apt, Bi, Cpx (29), Flds (44), Hb, Ol (32), Opx, Sp, W gabbro	Apt, Bi, Cpx (29), Flds (44), Hb, Ol (31), Opx, Sp, W gabbro	Amph, Apt, Bi, Cpx (40), Flds (24), Ol (0.4), Opx (7), Qtz, Sp, W gabbro
T magma final, °C	1143	1109	1112	1113	1116	1105	1107

[a]Amph–amphibole, Apt–apatite, Bi–biotite, Cpx–clinopyroxene, Flds–feldspatoids, Ilm–ilmenite, Gr–garnet, Hb–hornblende, liq.M–magma melt, liq.WR–anatectic melt, Ol–olivine, Opx–orthopyroxene, Qtz–quartz, Sp–spinel, Wtl–whitlockite, W–water, WR–wallrock.

olivine ($Fo_{82–86}$ mol%) and of 3 vol.% clinopyroxene phenocrysts [*Borisova et al*., 2002, 2014; *Weis et al*., 2002], and therefore clinopyroxene (cpx) to olivine ratio (cpx/olivine ratio) is close to zero. Melt inclusions interpreted as assimilant have SiO_2 contents of 49.5 ± 1.1 wt. % and relatively high K_2O/P_2O_5 (7.2 ± 4.4, Table 1). Selected input and output for the sixty seven MCS models are summarized in Tables 2 and 3 and additional information is provided in the supporting information Table S1 and Data Set S1. These models illustrate the sensitivity of recharge assimilation fractional crystallization (RAFC) of different wallrock

compositions, the impact of recharge, including variable number of recharge events (and this variable total mass of recharge magma added to the magma system), and varying pressure and water content. We also identify the fourteen best-fit simulations. Table 2 summarizes selected initial conditions for these models, and Table 3 provides results for each best-fit model, including the chemistry of wallrock liquid, a stable wallrock assemblage, and relevant masses.

Assimilation of IIb-type gabbro (GM 92–412, Models 1–5) [*Grégoire et al*., 2001] without any recharge produces wallrock liquids that trigger intensive clinopyroxene crystallization (from ~16 to 31 wt.%, where % is calculated on the basis of the initial starting mass of the magma) in the parental magma chamber at 0.2 GPa (Models 1–5; Tables 2 and 3; supporting information Table S1). Changing the initial temperature of wallrock does not improve model outcomes. Increasing water contents from 2 to 3 wt.% at 0.2 GPa (Model 6) decreases clinopyroxene and increases olivine abundance, yielding lower cpx/olivine ratios (compare Model 5 with 2 wt. % H_2O, cpx/olivine=4.3 and Model 6 with 3 wt. % H_2O, cpx/olivine=2.5), but the ratios are still much higher than observed in the Kerguelen samples. Models 7–9, which utilize a different wallrock composition (IIa/c GM 92–394), are also characterized by relatively high clinopyroxene abundances (~18 to 24 wt. %). A first order conclusion from models 1–9, which have cpx/olivine of 0.9 to 8.6, is that assimilation and fractional crystallization (AFC) models yield magmas in which clinopyroxene dominates over olivine, which is inconsistent with the observed mineral relationships of the 21 Ma host olivine-cumulative basalts.

Models 10 through 14 include one recharge event with different recharge masses (from a ratio of 1:1 initial magma body mass to recharge mass to a ratio of 1:0.5) and utilize IIa/IIc (GM 92–394) as the wallrock. The pressure is 0.2 GPa. These RAFC models yield cpx/olivine ratios from 1.3 to 3.6, compared to 4.5 obtained without recharge events at the same physico-chemical conditions (i.e., Model 8). Application of different wallrock metagabbro (IIb-type GM 139 and MG 134) [*Grégoire et al*., 1998] in Models 15 through 18 produces different cpx/olivine ratios from 4.7 to 2.5, respectively, that are still elevated compared to the observed ratio. Thus, like the AFC only models, crystallization of the olivine-saturated Plume melt accompanied by assimilation of different metagabbros (types IIa, b, and c) with a single recharge event (RAFC) favors clinopyroxene crystallization in the contaminated parental magma chamber at 0.2 GPa.

What conditions do favor an olivine dominated melt? An obvious possibility that produces better agreement between modeled and observed mineralogy of the olivine basalts (predominance of olivine above clinopyroxene phenocrysts) is larger recharge masses, where the recharge composition is that of the olivine-saturated Plume melt and the wallrock is Type IIb (MG 134) (Table 1 and supporting information Table S1). For example, increasing the number of recharge events from 1 to 4 (and therefore increasing the total magma:recharge ratio to 1:4; see next paragraph for discussion) in Models 18 through 22 results in a progressive decrease in the clinopyroxene to olivine ratio from 2.5 to 0.0. Similarly, increasing the number of recharge events from 1 to 4 (magma:recharge ratio to 1:4) in Models 31 through 34 (wallrock is Type IIb MG 139) decreases cpx/olivine ratio from 4.7 to 0.9. Additional groups of models (e.g., 35–38, 42–45) yield similar outcomes. The models discussed above illustrate the importance that magma recharge has on the evolution of Kerguelen basalt. While Tables 2 and 3 and supporting information Table S1 report multiple recharge events (up to 4 with individual magma:recharge ratios of 1:1), the most critical outcome of this analysis is the total (minimum) ratio of mass of magma to mass of recharge magma added to the system; best-fit results suggest this ratio is 1:4. The number of recharge events is more difficult to quantify. While four recharge events were modeled, a different number of events is equally plausible, as is continuous recharge. In each MCS model where more than one recharge event was modeled, the amount of crystallization (and associated cooling) that occurred between "events" was minimal (e.g., magma cooled at most 10s of degrees and the percent olivine crystallized is typically <5). What this suggests is that, compared to crystallization (and associated magma cooling), recharge was the dominant process required to generate the observed olivine-dominated magmas and the magma:recharge mass ratios were relatively high (see supporting information Table S1 for details regarding final magma temperature, total mass of cumulates, and total relative mass of recharge). Although beyond the scope of this contribution, constraints on the number of recharge events might be gleaned from zoning characteristics of minerals.

Additional models presented in Tables 2 and 3 and the supporting information Table S1 and Data Set S1 further illustrate the impact that variable pressure, initial water content of parent and recharge magmas, and wallrock composition have on the composition and mineralogy of the Kerguelen basaltic series. How sensitive are the models to pressure? A model run at significantly higher pressure does not enhance olivine stability. Model 15p,

run at 1 GPa, favors clinopyroxene and produces no olivine. Models 28, 29, and 30, run at 0.3 GPa, and involved IIb wallrock and four recharge events (where the magma:recharge mass ratios were 1:1, 1:0.75, 1:0.5, respectively); they yield cpx/olivine of 0.8, 1.5 and 2.5, respectively. At higher pressure (e.g., 0.3 GPa in the Models 28, 29, 30), the anatectic liquids can be more saturated in clinopyroxene molecule compared to those generated at 0.2 GPa (e.g., Model 24). Thus, even with four recharge events that might favor the formation of olivine over clinopyroxene, the 0.3 GPa models yield cpx/olivine ratios that are higher than comparable 0.2 GPa simulations.

It is well known that increased water content in basaltic melts is favorable for expansion of the olivine crystallization field compared to the clinopyroxene one [*Nicholls and Ringwood*, 1973]. Thus, the effect of higher H_2O (3 wt.% as compared to 2.0 wt.%) in the Plume melt (both parent magma and recharge magmas) was examined and is reported in all "w"-marked MCS models (e.g., 15w, 23w, 24w, 28w, 34w, 38w, 48w, 51w and 52w). This higher H_2O concentration is in accordance with representative H_2O contents in the Kerguelen plume magmas investigated experimentally [e.g., *Freise et al*., 2009] and based on glassy melt inclusions [*Borisova et al*., 2002]. These models have variable numbers of recharge events (typically between 3 and 4) and have cpx/olivine ratios of 0.4 to 0 (Figure 5). Thus, in all of these simulations, olivine dominates over clinopyroxene, highlighting the critical importance hydrous basalt (both as parent magma and recharge magmas) played in the evolution of the Kerguelen basalts. Several models that involve three to four recharge events (e.g., 22–30, 15w, 24w, 28w, 34w, 52w; magma:recharge mass ratios typically 1:3 to 1:4) with IIb-type wallrocks at 0.2–0.3 GPa reproduce the host basalt mineralogy (olivine $\gg$ clinopyroxene, Figure 5 and Table 3) as well as the composition of the magma liquids (Figures 3 and 4) accompanied by olivine ($Fo_{81–84}$ mol%) similar to that of the Kerguelen Plume melt hosted by Fo ($Fo_{82–86}$, Table 1). A lack of correlation between the major element and Pb isotopic features of the investigated natural melts (Figure 6a) may be partially explained by decoupling of elemental versus isotopic diffusional exchange happening during a binary mixing events established experimentally [e.g., *Lesher*, 1994]. It is important to note that in several models applying IIb-type metagabbro wallrock, the chemistry of the generated anatectic liquids matches the compositional range of both the Assimilant and Model Crustal Assimilant melts (Figures 3–6; Tables (1–3)). As noted, the wallrock melt liquid composition (e.g., low P_2O_5 down to 0.01 wt. %, Table 3 and Figure 4) produced by MCS modeling shares compositional similarities with the chemistry of both the Assimilant and Model Crustal Assimilant, both of which are mafic melts (Figures 3 and 5).

For example, Figures 3–6 demonstrate the best fit model (e.g., Model 28w), which uses IIb-type wallrock and has 4 recharge events (with the temperature of the magma between 1152 and 1155°C when recharge occurs, magma:recharge mass ratio 1:4) of hydrous Plume melt with a liquidus temperature of 1175°C. In the model, the wallrock liquid composition approaches that of the Assimilant and Model Crustal Assimilant (Figures 3 and 4, and 6). Figures 3 and 4 demonstrate that the modeled wallrock-derived liquids are also chemically similar to some of the glassy basaltic background (basaltic matrix) melts in theoretical equilibrium with $Fo_{78–75}$ [*Borisova et al*., 2014]. It is therefore likely that the Assimilant melts which have been found entrapped in the $Fo_{82–83}$ olivine may be formed by binary mixing between the wallrock-derived liquids and the Plume melts mostly entrapped in olivine of $Fo_{82–86}$. Moreover, a modest discrepancy (of 20 to 60°C) between the temperature range estimated by MCS for the liquids and that obtained by the melt inclusion homogenization for Plume and Assimilant melts (Table 1 and Figure 3) is likely related to volatile (e.g., H_2O) loss during the experimental heating of natural melt inclusions, resulting in an overestimation of the homogenization temperature compared to the real melt entrapment temperature. We also note that the initial temperatures of the wallrock are typically within 25°C degrees of the wallrock solidus (Table 3 and supporting information Table S1). Such initial wallrock temperatures are required in order to reproduce the observed combination of whole rock and olivine characteristics. This modeling outcome suggests that the wallrock was thermally primed by magmatism that preceded those recorded in the studied samples. Thus, best fit model 28w represented on Figures (3 and 4), and 6, involves hydrous Plume melt and IIb-type K-rich metagabbro (MG 134) wallrock melting at 0.3 GPa (Figure 4). Some discrepancy with respect to K_2O contents and K_2O/P_2O_5 ratios between the wallrock liquids relatively poor in K_2O and the Assimilant melts enriched in K_2O may be explained by more alkali-depleted character of the investigated crustal xenolith (IIb-type, MG 134) compared to an initial K-enriched chemistry before the crustal melting events. For example, the chemistry of other metagabbro (IIa-type, ARC 343, Model 48w, Figure 6b) may reflect such an initial K-Al-rich composition. We suggest that multiple episodes of partial melting and mixing event(s) in the mafic crust result in disappearance of mineral phases richest in alkalis, which produces more alkali-depleted crustal xenoliths such as MG 134.

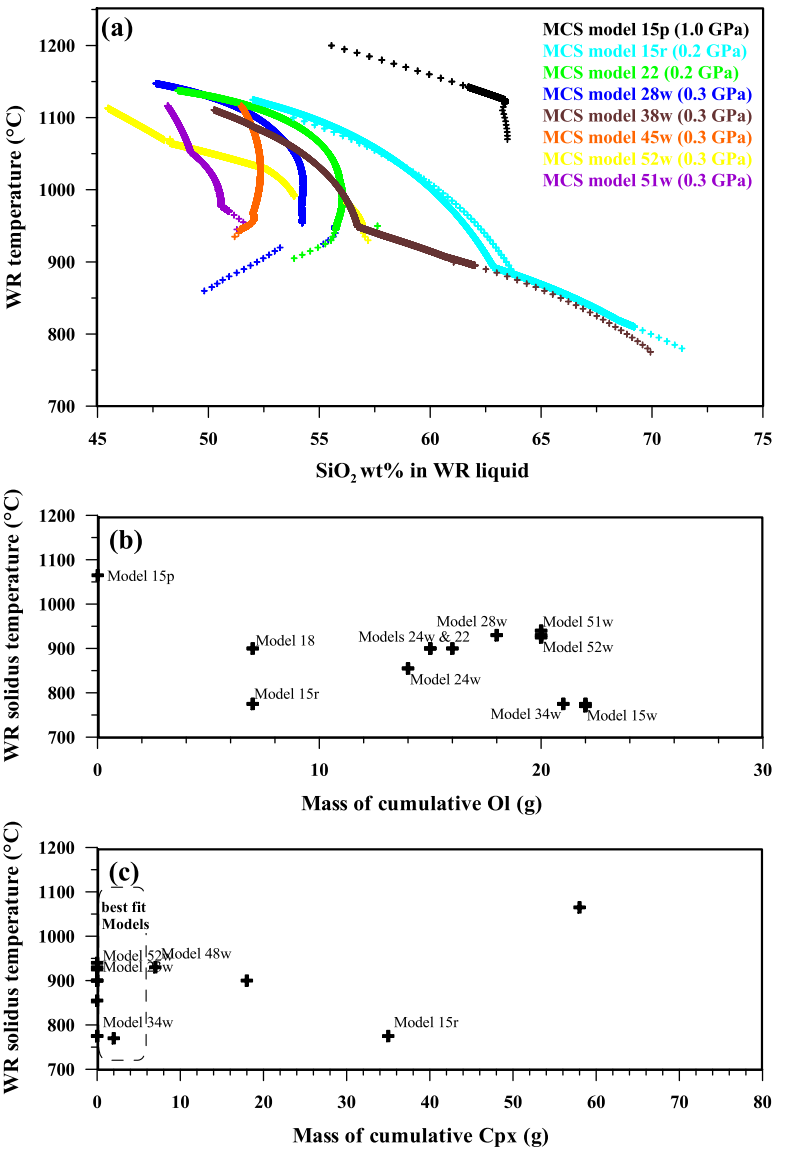

Figure 5. (a) The wallrock (WR) temperature versus SiO_2 wt.% content in the WR liquid for the best fit MCS models. (b) The wallrock (WR) solidus temperature versus Mass of cumulative olivine (Ol) in grams for the magma modeled by the Magma Chamber Simulator code for the best fit MCS models. (c) WR solidus temperature versus Mass of cumulative clinopyroxene (Cpx) in grams for the magma modeled by the Magma Chamber Simulator code for the best fit MCS models. In the performed MCS models, different wallrock compositions have been applied. Models with the mass of the cumulative clinopyroxene lower than 6 wt% are selected as the best fit (supporting information Table S1; Data Set S1).

4. Implication for Crustal Assimilation by Primitive OIB

The discovery of huge Pb isotope heterogeneity within olivine-hosted melt inclusions in basalts from Kerguelen, Iceland, Hawaii and the South Pacific Polynesia islands (Figure 1) implies not only mantle heterogeneities but also open-system behavior of OIBs, where during magma residence and transport, basaltic melts are contaminated by surrounding lithosphere. The Magma Chamber Simulator modeling developed in this work for the Kerguelen basaltic series illustrates how assimilation of metagabbro can affect typical primitive plume-derived melts. Our thermodynamic modeling using Magma Chamber Simulator predicts crustal metagabbro wallrock assimilation at 0.2–0.3 GPa, corresponding to a middle crustal parental basaltic magma chamber located at depths of 6–9 km at levels (Figure 3). Assimilation of crustal metagabbros by primitive OIB melts should be facilitated by the thermal influence of the mantle plume-derived magmas raising the temperature of the wallrocks, which eventually reach their solidi (770–940°C). Because the rate

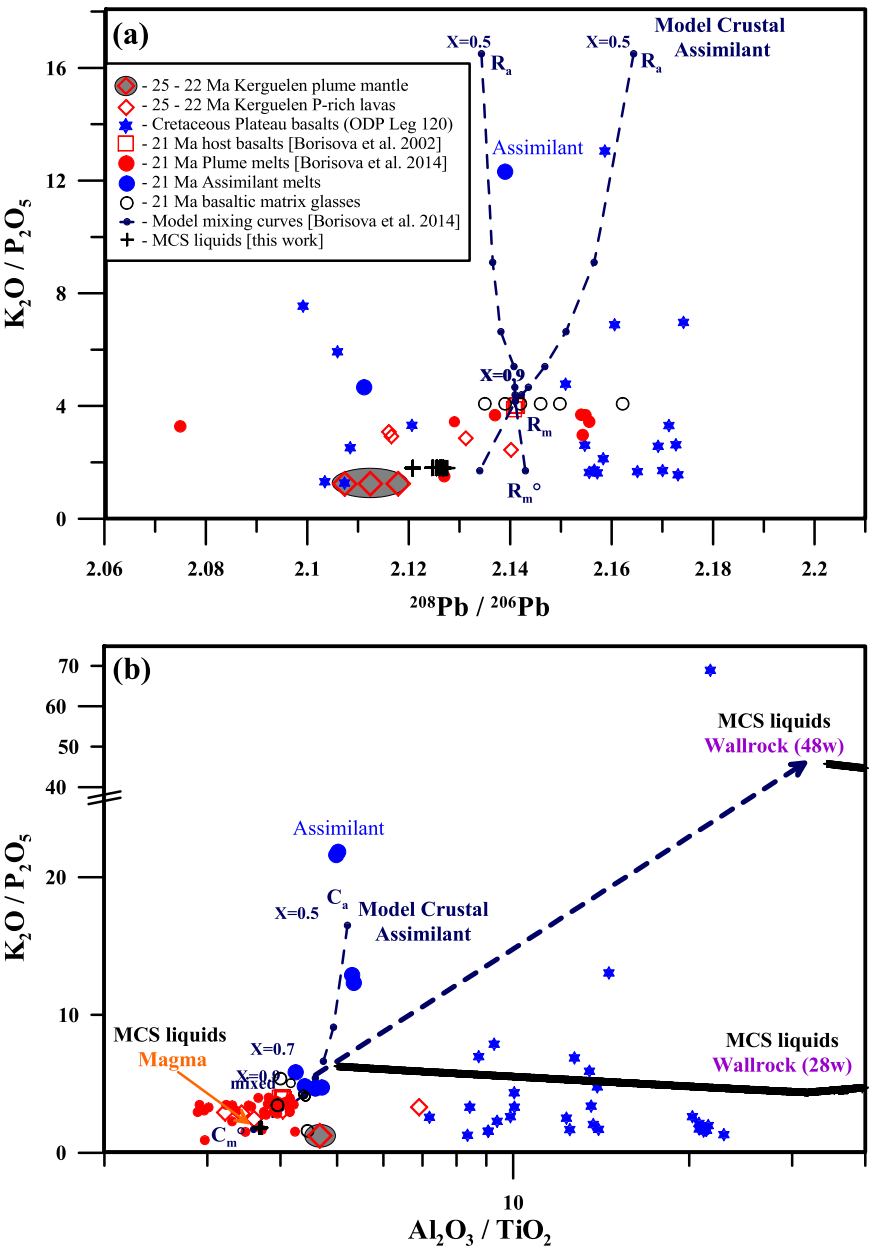

Figure 6. (a-b). (a) K_2O/P_2O_5 versus $^{208}Pb/^{206}Pb$, (b) K_2O/P_2O_5 versus Al_2O_3/TiO_2 measured in olivine phenocryst-hosted melt inclusions of the 21–19 Ma Kerguelen basaltic series. The isotopic and major element compositions of the basaltic melt inclusions are compared to those of the host basalts and the 25–22 Ma Kerguelen plume-derived basalts and P-rich lavas (grey field and open red diamond). "21 Ma Plume melts," "21 Ma Assimilant melts" and "21 Ma basaltic groundmass glasses" correspond to Plume, Assimilant melts and matrix glasses according to *Borisova et al.* [2002, 2014], respectively. The mixing lines corresponds to those modeled to get the composition of the Model Crustal Assimilant [*Borisova et al.*, 2014]. $^{208}Pb/^{206}Pb$ ratios measured in situ by LA-MC-ICP-MS and SIMS for the inclusion and matrix are compared to those of the bulk 21 Ma basalt, and other Kerguelen plume-derived (P-rich) lavas and the Cretaceous Kerguelen Plateau basalts. The basaltic lava data are from *Weis et al.* [2002]. Cretaceous Kerguelen Plateau basalt data are from *Frey et al.* [2002a]. The 25–22 Ma Kerguelen plume composition corresponds to that of *Weis and Frey* [2002] and *Frey et al.* [2002b] for $^{208}Pb/^{206}Pb$ ratio and to the data of *Frey et al.* [2002b] for the bulk-rock major element composition. The Magma Chamber Simulator (MCS) parental magma (Magma) liquids of 28w model are demonstrated. The Magma Chamber Simulator (MCS) wallrock (WR) liquids of two of the best fit 28w and 48w models are also demonstrated. The dashed arrows to higher values of Al_2O_3/TiO_2 and K_2O/P_2O_5 indicate the effect of crustal assimilation on the composition of the 21–19 Ma Kerguelen OIB basaltic series.

of heat diffusion in crustal rocks is considered to be high [e.g., *Chapman and Furlong*, 1992], the metagabbroic wallrock material is likely to reach its solidus temperature relatively rapidly upon the magma-wallrock interaction, especially in the case of relatively large input of recharge magma. The OIB magma–oceanic

crust interaction is expressed by effective partial melting of the metagabbro xenoliths, starting at solidus conditions (770 – 940°C at 0.2 – 0.3 GPa), with predominant consumption of plagioclase and clinopyroxene from the wallrocks. The MCS modeling also predicts that assimilation of metagabbro-derived partial anatectic melts are clinopyroxene-saturated at the middle crustal conditions, and thus assimilation favors clinopyroxene crystallization in the parental basaltic magma chamber. Thus, the anatectic melts are saturated in clinopyroxene in accordance with the conclusion of *Gurenko and Sobolev* [2006]. The partial melts, however, can progressively become olivine-saturated upon their mixing with predominantly olivine-saturated recharge melts. We suggest that the percolating anatectic melts progressively lose their initial major, trace element and isotopic features, e.g., Sr enrichment [*Gurenko and Sobolev*, 2006] and can progressively acquire a "ghost plagioclase signature" [*Sobolev et al*., 2000].

For the 21 Ma Kerguelen OIB case, crustal assimilation was accompanied by minor crystallization of clinopyroxene and predominant growth of olivine phenocrysts with chromiferous spinel from heterogeneous melts of OIB basaltic magma at preeruptive middle crustal conditions (e.g., 1105–1143°C and 0.2–0.3 GPa). Our data imply that similarly to the investigated case of the 21 Ma olivine-cumulative basalts from Kerguelen hot spot, the primitive OIB magmas are olivine-phyric due to multiple recharge events of mantle plume-derived olivine-saturated basaltic melts. Moreover, an addition of an EM-1-type assimilant from an oceanic (subcontinental) lithosphere (e.g., middle-lower mafic crust) altered by circulating seawater-derived fluids to the mantle-derived OIB magma could result in decrease in $\delta^{18}O$ and $^{206}Pb/^{204}Pb$ ratio in the crystallizing minerals and the host hybrid magma [e.g., *Eiler*, 2001; *Borisova et al*., 2001; *Frey et al*., 2002a; *Bindeman*, 2008 and references therein; *Gurenko et al*., 2015]. The process may be established based on *in-situ* microanalytical study of the OIB mineral and glass phases such as the mineral-hosted glass inclusions [e.g., *Borisova et al*., 2014; *Gurenko et al*., 2015, and references therein] rather than the bulk-rock OIB composition because a mixed signature of the crustal and mantle events.

In summary, our model for the primitive OIB thus requires (1) presence of a middle crustal (0.2–0.3 GPa) rather than deep lithospheric (1.0 GPa) magma chamber systems for the investigated primitive olivine-phyric OIB basaltic series. (2) Olivine-saturated OIB melts are produced through crustal metagabbro assimilation (up to ~30 wt. %) by mixing between the wallrock-derived anatectic and parental melts in combination with multiple episodes of recharge of hydrous olivine-saturated primitive basaltic melts. (3) The chemistry of the produced primitive OIBs, thus, strongly depends on whether the parental magma has resided in the gabbroic crust, and on the efficacy of crustal assimilation. We believe that the chemistry of the OIB is also determined by the timescale of the parental magma residence in the gabbroic crust. The combination of effective crustal assimilation with multiple episodes of recharge of plume melts implies that the bulk-rock OIB composition (chemistry and isotopic composition) represents some average of the mantle-derived and crustal melts.

Acknowledgments
Authors thank Associate Editor Janne Blichert-Toft, and reviewers Ilya Bindeman, Leif Karlstrom, Frances Jenner and anonymous reviewers for important suggestions on the previous versions of the manuscript. Vladimir K. Illarionov is thanked by A.Y.B. for discussion on the current work. A.Y.B. thanks INSU (France) 2014–2015 for the financial support of this work and her stay at the Central Washington University (USA). Development of the Magma Chamber Simulator was supported by grants from the US National Science Foundation. The Excel data set describing the characteristics of all Magma Chamber Simulator models performed in this work is available in the supporting information.

References

Allegre, C. J. (1982), Chemical geodynamics, *Tectonophysics*, *81*, 109–132.
Ashwal, L. D., M. Wiedenbeck, and T. H. Torsvik (2017), Archaean zircons in Miocene oceanic hotspot rocks establish ancient continental crust beneath Mauritius, *Nat. Commun.*, *8*, 14086, doi:10.1038/ncomms14086.
Bindeman, I. (2008), Oxygen isotopes in mantle and crustal magmas as revealed by single crystal analysis, *Rev. Mineral. Geochem.*, *69*, 445–478.
Bindeman, I. N., O. Sigmarsson, and J. Eiler (2006), Time constraints on the origin of large volume basalts derived from O-isotope and trace element mineral zoning and U-series disequilibria in the Laki and Grímsvötn volcanic system, *Earth Planet. Sci. Lett.*, *245*, 245–259.
Bindeman, I. N., A. Gurenko, O. Sigmarsson, and M. Chaussidon (2008), Oxygen isotope heterogeneity and disequilibria of olivine crystals in large volume Holocene basalts from Iceland: Evidence for magmatic digestion and erosion of Pleistocene hyaloclastites, *Geochim. Cosmochim. Acta*, *72* (17), 4397–4420.
Bohrson, W. A., F. J. Spera, M. S. Ghorso, G. A. Brown, J. B. Creamer, and A. Mayfield (2014), Thermodynamic model for energy-constrained open-system evolution of crustal magma bodies undergoing simultaneous recharge, assimilation and crystallization: The Magma Chamber Simulator, *J. Petrol.*, *55*, 1685–1717.
Borisova, A. Y., B. V. Belyatsky, M. V. Portnyagin, and N. M. Sushchevskaya (2001), Petrogenesis of olivine-phyric basalts from the Aphanasey Nikitin Rise: Evidence for contamination by cratonic lower continental crust, *J. Petrol.*, *42*, 277–319.
Borisova, A. Y., I. K. Nikogosian, J. Scoates, D. Weis, D. Damasceno, N. Shimizu, and J. L. R. Touret (2002), Melt, fluid and crystal inclusions in olivine phenocrysts from Kerguelen plume-derived picritic basalts: Evidence for interaction with the Kerguelen Plateau lithosphere, *Chem. Geol.*, *183*, 195–220.
Borisova, A. Y., G. Ceuleneer, S. Arai, V. Kamenetsky, F. Béjina, M. Polvé, Ph. de Parseval, T. Aigouy, and G. S. Pokrovski (2012), A new view on the petrogenesis of the Oman ophiolite chromitites from microanalyses of chromite-hosted inclusions, *J. Petrol.*, *53*(12): 2411–2440, doi:10.1093/petrology/egs054.
Borisova, A. Y., F. Faure., E. Deloule., M. Grégoire, F. Béjina, Ph. de Parseval, and J.-L. Devidal (2014), Lead isotope signatures of Kerguelen plume-derived olivine-hosted melt inclusions: Constraints on the ocean island basalt petrogenesis, *Lithos*, *198–199*, 153–171, doi: 10.1016/j.lithos.2014.03.022.

Chapman, D. S., and K. P. Furlong (1992), Thermal state of the continental lower crust, in, *Continental Lower Crust, Developments in Geotectonics*, vol. 23, edited by D. M. Fountain and R. R. W. Arculus Kay, Elsevier, pp. 179–199, Amsterdam.
Danyushevsky, L. V., A. W. McNeill, and A. V. Sobolev (2002), Experimental and petrological studies of melt inclusions in phenocrysts from mantle-derived magmas: An overview of techniques, advantages and complications, *Chem. Geol.*, *183*(1–4), 5–24.
Edwards, B. R., and J. K. Russell (1998), Time scales of magmatic processes: New insights from dynamic models for magmatic assimilation, *Geology*, *26*(12), 1103–1106.
Eiler, J. M. (2001), Oxygen isotope variations in basaltic lavas and upper mantle rocks, *Rev. Mineral. Geochem.*, *43*, 319 – 364.
Freise, M., F. Holtz, M. Nowak, J. S. Scoates, and H. Strauss (2009), Differentiation and crystallization conditions of basalts from the Kerguelen large igneous province: An experimental study, *Contrib. Mineral. Petrol.*, *158* (4), 505–527.
Frey, F. A., et al. (2000), Origin and evolution of a submarine large igneous province: The Kerguelen Plateau and Broken Ridge, southern Indian Ocean, *Earth Planet. Sci. Lett.*, *176*, 73–89.
Frey, F.A., D. Weis, A. Y. Borisova, and G. Xu (2002a), Involvement of continental crust in the formation of the Kerguelen Plateau: New perspectives from ODP Leg 120 Sites, *J. Petrol.*, *43*, 1207–1239.
Frey, F. A., K. Nicolaysen, B. K. Kubit, D. Weis, and A. Giret (2002b), Flood basalt from Mont Tourmente in the Central Kerguelen Archipelago: The change from transitional to alkali basalt at 25 Ma, *J. Petrol.*, *43*(7), 1367–1387.
Frey, F. A., I. G. N. Silva, S. Huang, M. S. Pringle, P. R. Meleney, and D. Weis (2015), Depleted components in the source of hotspot magmas: Evidence from the Ninetyeast Ridge (Kerguelen), *Earth Planet. Sci. Lett.*, *426*, 293 – 304.
Gautier, I., D. Weis, J. P. Mennessier, P. Vidal, A. Giret, and M. Loubet (1990), Petrology and geochemistry of the Kerguelen Archipelago basalts (South Indian Ocean)-Evolution of the mantle sources from ridge to intraplate position, *Earth Planet. Sci. Lett.*, *100*, 59–76.
Genske, F. S., C. Beier., K. M. Haase, S. P. Turner, S. Krumm., and P. A. Brandl (2014), Oxygen isotopes in the Azores islands: Crustal assimilation recorded in olivine, *Geology*, *41*, 491–494, doi:10.1130/G33911.1.
Grégoire, M., N. Mattielli, C. Nicollet, J.-Y. Cottin, H. Leyrit, D. Weis, N. Shimizu, and A. Giret (1994), Oceanic mafic granulite xenoliths from the Kerguelen Archipelago, *Nature*, *367*(6461), 360–363.
Grégoire, M., J.-P. Lorand, J.-Y. Cottin, A. Giret, N. Mattielli, and D. Weis (1997), Xenoliths evidence for a refractory oceanic mantle percolated by basaltic melts beneath the Kerguelen archipelago, *Eur. J. Mineral.*, *9*, 1085–1100.
Grégoire, M., J.-Y. Cottin, A. Giret, N. Mattielli, and D. Weis (1998), The meta-igneous granulite xenoliths from Kerguelen Archipelago: Evidence of a continent nucleation in an oceanic setting, *Contrib. Mineral. Petrol.*, *133*(3), 259–283.
Grégoire, M., I. Jackson., S. Y. O'Reilly, and J. Y. Cottin (2001), The lithospheric mantle beneath the Kerguelen Islands (Indian Ocean): Petrological and petrophysical characteristics of mantle mafic rock types and correlation with seismic profiles, *Contrib. Mineral. Petrol.*, *142*, 244–259.
Gurenko, A. A., and A. V. Sobolev (2006), Crust-primitive magma interaction beneath neovolcanic rift zone of Iceland recorded in gabbro xenoliths from Midfell, SW Iceland, *Contib. Mineral. Petrol.*, *151*, 495–520.
Gurenko, A. A., I. N. Bindeman, and I. A. Sigurdsson (2015), To the origin of Icelandic rhyolites: insights from partially melted leucocratic xenoliths, *Contrib. Mineral. Petrol.*, *169*, 49, doi:10.1007/s00410-015-1145-4.
Hart, S. (1984), The large-scale isotope anomaly in the Southern Hemisphere mantle, *Nature*, *309*, 753–757.
Hilton, D. R., J. Barling, and G. E. Wheller (1995), Effect of shallow-level contamination on the helium isotope systematics of ocean–island lavas, *Nature*, *373*(6512), 330–333.
Kamenetsky, V. S., and A. A. Gurenko (2007), Cryptic crustal contamination of MORB primitive melts recorded in olivine-hosted glass and mineral inclusions, *Contrib. Mineral. Petrol.*, *153*, 465–481.
Kamenetsky, V. S., R. Maas, N. M. Sushchevskaya, M. D. Norman, and A. A. Peyve (2001), Remnants of Gondwanan continental lithosphere in oceanic upper mantle: Evidence from the South Atlantic Ridge, *Geology*, *29*(3), 243–246.
Kobayashi, K., R. Tanaka, T. Moriguti, K. Shimizu, and E. Nakamura (2004), Lithium, boron, and lead isotope systematics of glass inclusions in olivines from Hawaiian lavas: Evidence for recycled components in the Hawaiian plume, *Chem. Geol.*, *212*, 143–161.
Kvassnes, A. J. S., and T. L. Grove (2008), How partial melts of mafic lower crust affect ascending magmas at oceanic ridges, *Contrib. Mineral. Petrol.*, *156*, 49–71.
Lesher, C. E. (1994), Kinetics of Sr and Nd exchange in silicate liquids: Theory, experiments, and applications to uphill diffusion, isotopic equilibration, and irreversible mixing of magmas, *J. Geophys. Res.*, *99*(B5), 9585–9604.
MacLennan, J., (2008), Lead isotope variability in olivine-hosted melt inclusions from Iceland, *Geochim. Cosmochim. Acta*, *72*(16), 4159–4176.
Mattielli, N. (1996), Magmatism and metasomatism associated with the Kerguelen Plume: Contribution of geochemical characteristics from basic and ultrabasic xenoliths, Thèse de Doctorat., pp. 200,Univ. Libre de Bruxelles, Bruxelles, Belgium.
Mattielli, N., D. Weis, J. S. Scoates, N. Shimizu, J.-P. Mennessier, M. Grégoire, J.-Y. Cottin, and A. Giret (1999), Evolution of heterogeneous lithospheric mantle in a plume environment beneath the Kerguelen Archipelago, *J. Petrol.*, *40*, 1721–1744.
McDonough, W. F., and S. S. Sun (1995), The composition of the Earth, *Chem. Geol.*, *120*, 223–253.
Nicholls, I. A., and A. E. Ringwood (1973), Effect of water on olivine stability in tholeiites and the production of silica-saturated magmas in the island-arc environment, *J. Geol.*, *81*, 285–300.
Nicolaysen, K., F. A. Frey, K. V. Hodges, D. Weis, and A. Giret (2000), Ar-40/Ar-39 geochronology of flood basalts from the Kerguelen Archipelago, southern Indian Ocean: Implications for Cenozoic eruption rates of the Kerguelen plume, *Earth Planet. Sci. Lett.*, *174*, 313–328.
Olierook, H. K. H., R. E. Merle, and F. Jourdan (2017), Toward a Greater Kerguelen large igneous province: Evolving mantle source contributions in and around the Indian Ocean, *Lithos*, *282–283*, 163–172.
Paul, B., J. D. Woodhead, J. Hergt, L. Danyushevsky, T. Kunihiro, and E. Nakamura (2011), Melt inclusion Pb-isotope analysis by LA–MC-ICPMS: Assessment of analytical performance and application to OIB genesis, *Chem. Geol.*, *289*(3–4), 210–223.
Recq, M., D. Brefort, J. Malod, and J.-L. Veinante (1990), The Kerguelen Isles (southern Indian Ocean): New results on deep structure from refraction profiles, *Tectonophysics*, *182*(3), 227–248.
Saal, A. E., S. R. Hart, N. Shimizu, E. H. Hauri, and G. D. Layne (1998), Pb isotopic variability in melt inclusions from oceanic island basalts, Polynesia, *Science*, *282*, 1481–1484.
Saal, A. E., S. R. Hart, N. Shimizu, E. H. Hauri, G. D. Layne, and J. M. Eiler (2005), Pb isotopic variability in melt inclusions from the EMI–EMII–HIMU mantle end-members and the role of the oceanic lithosphere, *Earth Planet. Sci. Lett.*, *240*(3–4), 605–620.
Scoates, J. S., D. Weis, M. Franssens, N. Mattielli, H. Annell, F. A. Frey, K. Nicolaysen, and A. Giret (2008), The Val gabbro plutonic suite: A sub-volcanic intrusion emplaced at the end of Flood basalt magmatism on the Kerguelen Archipelago, *J. Petrol.*, *49*(1), 79–105.
Sobolev, A. V., A. W. Hofmann, and I. K. Nikogosian (2000), Recycled oceanic crust observed in "ghost plagioclase" within the source of Mauna Loa lavas, *Nature*, *404*, 986–990.

Sobolev, A. V., A. W. Hofmann, K. P. Jochum, D. V. Kuzmin, and B. Stoll (2011), A young source for the Hawaiian plume, *Nature*, *467*, 434–439.

Sun, S-S., and W. M. McDonough (1989), Chemical and isotope systematics of oceanic basalts: implications for mantle compositions and processes, in edited by A. D. Saunders, and M. J. Norry, *Magmatism in the Ocean Basins*, Geological Society Special London Publication 42, pp. 313–345.

Sushchevskaya, N. M., O. V. Levchenko, E. P. Dubinin, and B. V. Belyatsky (2015), Ninetyeast Ridge: Magmatism and geodynamics, *Geochem. Int.*, *54*, 237–256.

Torsvik, T. H., H. Amundsen, E. H. Hartz, F. Corfu, N. Kusznir, C. Gaina, P. V. Doubrovine, B. Steinberger, L. D. Ashwal, and B. Jamtveit (2013), A Precambrian microcontinent in the Indian Ocean, *Nat. Geosci.*, *6*, 223–227, doi:10.1038/ngeo1736.

Torsvik, T. H., et al. (2015), Continental crust beneath southeast Iceland, *Proc. Natl. Acad. Sci. U. S. A.*, E1818–E1827, doi:10.1073/pnas.1423099112.

Weis, D., and F. A. Frey (2002), Submarine basalts of the Northern Kerguelen Plateau: Interaction between the Kerguelen plume and the Southeast Indian Ridge revealed at ODP Site 1140, *J. Petrol.*, *43*(7), 1287–1309.

Weis, D., F. A. Frey, R. Schlich, M. Schaming, R. Montigny, D. Damasceno, N. Mattielli, K. E. Nicolaysen, and J. S. Scoates (2002), Trace of the Kerguelen mantle plume: Evidence from seamounts between the Kerguelen Archipelago and Heard Island, Indian Ocean, *Geochem. Geophys. Geosyst.*, *3*(6), 1033, doi:10.1029/2001GC000251.

Xia, Q-K., Y. Bi, P. Li, W. Tian, X. Wei, H-L. Chen (2016), High water content in primitive continental flood basalts, *Scientific Reports*, *6*, 25416, doi:10.1038/srep25416.

Yano, T., B. I. Vasiliev, D. R. Choi, S. Miyagi, A. A. Gavrilov, and H. Adachi. (2011), Continental rocks in the Indian Ocean, *New Concepts Global Tectonics Newsl.*, *58*, 9–28.

Yurimoto, H., et al. (2004), Lead isotopic compositions in olivine-hosted melt inclusions from HIMU basalts and possible link to sulfide components, *Phys. Earth Planet. Inter.*, *146*, 231–242.

Zindler, A., and S. Hart (1986), Chemical geodynamics, *Annu. Rev. Earth Planet. Sci.*, *14*, 493–571.